NIH Public Access
Author Manuscript
*Nat Struct Mol Biol*. Author manuscript; available in PMC 2010 August 17.

Published in final edited form as:
*Nat Struct Mol Biol*. 2008 January ; 15(1): 50–56. doi:10.1038/nsmb1350.

# Structural basis for synaptic adhesion mediated by neuroligin-neurexin interactions

**Xiaoyan Chen**[1], **Heli Liu**[1], **Ann H. R. Shim**[1], **Pamela J. Focia**[1], and **Xiaolin He**[1]

[1]Northwestern University Feinberg School of Medicine, Department of Molecular Pharmacology & Biological Chemistry, Searle 8-417, 303 East Chicago Avenue, Chicago, Illinois 60611, USA.

## Abstract

The heterophilic synaptic adhesion molecules, neuroligins and neurexins, are essential for establishing and maintaining neuronal circuits by modulating the formation and maturation of synapses. The neuroligin-neurexin adhesion is $Ca^{2+}$-dependent and regulated by alternative splicing. We report a 2.4Å structure of the complex between the mouse neuroligin-1 (NL1) cholinesterase-like domain and the mouse neurexin 1β (NX1β) LNS (laminins, neurexins, and sex hormone-binding globulin-like) domain. The structure reveals a delicate neuroligin-neurexin assembly mediated by a hydrophilic, $Ca^{2+}$-mediated, and solvent-supplemented interface, rendering it capable of being modulated by alternative splicing and other regulatory factors. Thermodynamic data support a mechanism where splicing site B of NL1 acts by modulating a salt bridge at the edge of the NL1-NX1β interface. Mapping neuroligin mutations implicated in autism indicates most such mutations are structurally destabilizing, supporting deficient neuroligin biosynthesis and processing as a common cause for this brain disorder.

## Introduction

The development of the central nervous system relies on specific cell-cell recognition and communication through synapses, the specialized junctions between neurons. At the synapse, presynaptic and postsynaptic membranes are linked together by a variety of adhesion molecules[1]. Two adhesion molecules that have been implicated in the establishment and maturation of synaptic contacts are neuroligins, which are postsynaptic proteins, and neurexins, which are presynaptic proteins[2–7]. Polymorphisms in neuroligin and neurexin genes have been associated with several cases of cognitive disorders such as autism and mental retardation[8–15].

Neuroligins are a family of four type I transmembrane proteins (neuroligins 1–4, or NL1-4), whose extracellular segments contain a globular domain homologous to acetyl-cholinesterase (AChE) and an O-linked carbohydrate-rich stalk[16]. The neurexin family consists of three genes, each generating a long mRNA encoding α-neurexin and a short mRNA encoding β-neurexin. The extracellular segment of α-neurexins contains six LNS domains, whereas β-neurexins contain a single LNS domain identical to the last one of α-

Correspondence should be addressed to X.H. (x-he@northwestern.edu).

**Accession code**. Protein Data Bank: Coordinates and structural factors have been deposited with accession code 3B3Q.

Note: Supplementary information is available on the Nature Structural & Molecular Biology website.

AUTHOR CONTRIBUTIONS

X.C., H.L., A.H.R.S. and P.J.F. carried out experiments; X.H. supervised the research; X.C. and X.H. wrote the paper.

COMPETING INTEREST STATEMENT

The authors declare no competing financial interests.

NIH-PA Author Manuscript
NIH-PA Author Manuscript
NIH-PA Author Manuscript

NIH-PA Author Manuscript

NIH-PA Author Manuscript

NIH-PA Author Manuscript

neurexins. The cholinesterase-like domain (CLD) of neuroligins and the common LNS domain between α- and β-neurexins are implicated in recognition[4,17]. The structure of the NX1β LNS domain has been determined[18]. The structure of neuroligins, and the overall arrangement of neuroligin and neurexin within the synapse, have been extensively studied by hydrodynamic and small angle scattering methods[19–21]. Neuroligin-neurexin binding is $Ca^{2+}$-dependent[22], but the exact position of the $Ca^{2+}$ binding site and the role of $Ca^{2+}$ binding in neuroligin-neurexin association have remained uncertain.

Both neuroligins and neurexins undergo extensive alternative mRNA splicing[16]. The CLD of neuroligins contains splice site A, and specifically in NL1, an additional splice site B. α-neurexins contain five splice sites, in which the fourth site (SS#4) is located in the common LNS domain of α- and β-neurexins. Both neuroligin splice sites and neurexin SS#4 have been shown to modulate synaptic recognition[20,23–27]. Previous small-angle scattering data[21] suggested these splice sites are central or proximal to neuroligin-neurexin interaction, but their exact positions relative to the neuroligin-neurexin interface, as well as the mechanism by which these sites modulate neuroligin-neurexin recognition, remained unclear. Here we report a 2.4Å resolution crystal structure of the complex between the CLD of mouse NL1 and the LNS domain of mouse NX1β, revealing the basis of neuroligin-neurexin recognition, and illuminating the mechanisms of regulation by factors such as $Ca^{2+}$ and alternative splicing.

## Results

### Confirmation of the functional unit of NL1-NX1β complex

To reconstitute the NL1-NX1β complex, we expressed the NX1β LNS domain and the NL1 CLD using baculovirus. Crystals of the complex were obtained with NL1 and NX1β combined in the presence of $Ca^{2+}$. The structure was determined by molecular replacement. The asymmetric unit contains two NX1β and two NL1. Because each NL1 is involved in crystal packing with four neighboring NX1β, it was unclear which pairs of NL1 and NX1β are the functional units. The interaction between neuroligins and neurexins has not been systematically mapped, despite existing mutagenesis data on both NL1 and NX1β[20,25]. To prevent misidentifying packing artifacts as functional interfaces, we studied all four NL1-NX1β crystal contacts, which bury surface areas of 1160 $Å^2$, 1030 $Å^2$, 560 $Å^2$, and 140 $Å^2$, respectively (Fig. 1 and Supplementary Fig. 1 online). We tested the two larger interfaces (#1 and #2) by designing five NX1β mutants (S107R, L135R, D137S, I236R, and N238R) within interface #1 and two NX1β mutants (R112E and T179A) within interface #2, and compared the NL1-binding capacities of the mutants and wild-type NX1β. His-tag pulldown experiments (Fig. 1a) indicated only the interface #1 mutations reduced NL1 binding. To further evaluate the importance of interface #1, we tested mutations (E397A and N400A) of two NL1 residues central to interface #1 and involved in multiple NL1-NX1β interactions. These NL1 mutants did not show detectable binding to wild-type NX1β in calorimetric experiments (Supplementary Fig. 2 online). The mutagenesis data therefore indicate that interface #1 (see the buried interfaces in Fig. 1) is physiologically relevant.

### Structure of the NL1-NX1β complex

The NL1-NX1β complex contains a central NL1 dimer and two NX1β monomers, one attached to each side (Fig. 1b and 1c). NL1 dimerization ensures NX1β clustering. The NL1 monomer contains a 550 amino acid, globularly shaped CLD, with a central 11-strand β-sheet flanked by α-helices. The NL1 dimer in the complex, as expected from its ~30% sequence identity to AChE[28], can be superimposed upon the mouse AChE dimer (rmsd 1.4 Å for Cα atoms) (Supplementary Fig. 3 online). The dimer interface of NL1, similar to AChE, is formed by four α-helices near the C-termini, with two helices (residues 450–460

NIH-PA Author Manuscript

NIH-PA Author Manuscript

NIH-PA Author Manuscript

and 620–635) from each monomer. The dimer interface is large, burying 1590 Å$^2$ of surface area, and is primarily hydrophobic. With the Met459-Met459 and Leu633-Leu633 contacts from both chains as the dividing line, the interface appears as a duplex of two equivalent sub-interfaces. Each sub-interface is marked by a central Phe458, surrounded by Trp463 and Met459 from its own monomer, and Met459, Leu625, Leu629 from the opposing monomer (Supplementary Fig. 3 online). The NX1β LNS domain is β-sandwich-like as previously described[18]. Each NX1β uses a loop-rich surface lying on the side of the β-sandwich, previously designated as the "hyper-variable surface"[18], to contact NL1, whereas NL1 uses the region around the exposed side of the central β-sheet to contact NX1β. With respect to the orientation of NX1β relative to NL1, the β-sheets of NX1β and the long axis of NL1 dimer are vertical, but not parallel as suggested in previous small angle scattering studies[21], to each other.

## The $Ca^{2+}$ binding site is in NX1β but also reliant on NL1

After refining the protein part of the structure, we searched the asymmetric unit for $Ca^{2+}$. Initially, our effort was compromised by the requirement of using sodium citrate, a known chelating reagent, at high concentration (~1M) for crystallization. Nevertheless, the SIGMAA-weighted composite omit 2Fo-Fc map and the protein-only Fo-Fc electron density map (Supplementary Fig. 4 online) revealed a unique site in each pair of NL1 and NX1β, surrounded by 4 NX1β oxygen atoms. The electron density for the site was modest. We speculated that it might be a $Ca^{2+}$ ion present at partial occupancy. Although the total $Ca^{2+}$ concentration was 10mM during crystallization, free $Ca^{2+}$ was estimated to be only ~$10^{-2}$ mM due to citrate chelation. We therefore speculated that citrate chelation competes with the $Ca^{2+}$ binding site, resulting in the low occupancy. To verify our speculations, we replaced citrate with acetate in the mother liquor before X-ray diffraction data were measured, and obtained a 3.5 Å dataset. After simple rigid-body refinement to accommodate cell-dimension differences, electron density maps were calculated using the data from the acetate-adapted crystal. Strong electron density at this position unambiguously revealed it is a $Ca^{2+}$ binding site (Fig. 2a and Supplementary Fig. 4 online).

The bound $Ca^{2+}$ has direct contacts only with NX1β, and not with NL1 as suggested previously[22]. The $Ca^{2+}$ binding site in NX1β is located at the hyper-variable surface. Coordination of the bound $Ca^{2+}$ is consistent with an octahedral geometry (n=6) (Fig. 2a), with two main-chain carbonyl oxygens (Val154 and Ile236) and two side-chain oxygens (Asp137 and Asn238) from NX1β, and two water molecules ligated to the $Ca^{2+}$. Although NX1β provides all the non-solvent oxygen atoms for the bound $Ca^{2+}$, we were unable to detect binding between $Ca^{2+}$ and uncomplexed NX1β using calorimetry (Supplementary Fig. 5 online), consistent with previous observations that $Ca^{2+}$ incubation did not induce structural change of NX1β[22], suggesting that $Ca^{2+}$ binding requires the presence of NL1. Analyzing the NL1-NX1β structure revealed that one of the water molecules in $Ca^{2+}$ coordination, WAT1, is hydrogen bonded to the main-chain carbonyl of Gln395 and the side-chain carboxyl of Glu397 from NL1, suggesting NL1 plays a role in $Ca^{2+}$ binding by coordinating this water molecule for the completion of the $Ca^{2+}$ binding site.

Superimposition of the structure of NX1β in our complex with the structure of NX1α-LNS2 [29] revealed that their calcium ions are bound at similar positions (Fig. 2b). Most structural elements for $Ca^{2+}$ coordination are conserved, except that one water molecule in NX1α-LNS2 is replaced with the amide carbonyl from NX1β Asn238. Since the NX1α-LNS2 $Ca^{2+}$ binding site includes more water molecules, it is surprising that NX1α-LNS2 alone binds $Ca^{2+}$ at measurable affinity (~400μM)[29], but NX1β alone does not show detectable $Ca^{2+}$ binding. One explanation may be the differences in localizing these water molecules, especially the one at the NX1β WAT1 position (Fig. 2b).

NIH-PA Author Manuscript

NIH-PA Author Manuscript

NIH-PA Author Manuscript

### The interface between NL1 and NX1β

The NL1-NX1β interface contains a protruding surface patch at the edge of central β-sheet of NL1 and part of the hyper-variable surface of NX1β (Fig. 3). The majority of the interface on NL1 side emanates from loop 395–402, a smaller fraction from the short, flanking loop 499–502, and a minor fraction from sidechains extending from loop 292–310 and loop 380–388. The NX1β side of the interface consists of two long, parallel loops (101–110 and 231–241) and a short loop (131–137). The 1160 $Å^2$ total buried solvent-accessible surface area between each pair of NX1β and NL1 is smaller than the average of 1600±400 $Å^2$ expected for protein-protein interfaces[30]. The interface is primarily composed of hydrophilic residues. The only interactions between hydrophobic residues are between NX1β Leu135 and NL1 Phe499, and between NX1β Ile236 and NL1 Leu399. A total of 6 direct hydrogen bonds are formed between NL1 and NX1β, mostly contributed by only two residues, Glu397 and Asn400, from NL1 (Fig. 3). Mutations of either residue to alanine (E397A or N400A) abolished NL1-NX1β binding, confirming their essential roles (Supplementary Fig. 2 online). At the edge of the interface, two salt bridges are formed between NL1 Asp387 and NX1β Arg232, and between NL1 Glu297 and NX1β Arg109. Notably, these two salt bridges are not grouped with other interactions, and therefore are not reinforced by the adjacent structural elements. Water molecules fill in the unoccupied space between the opposing surfaces of NX1β and NL1, with some forming hydrogen bonds with both molecules. The hydrophilic and water-supplemented nature of NL1-NX1β interface is consistent with previous studies showing that NL1-NX1β binding affinity is inversely related to the ionic strength of the solution[19].

### Specificity of neuroligin-neurexin interactions

The ranking order of neuroligins toward binding NX1β is NL1>NL4≫NL3>NL2[20]. Sequence alignment of neuroligins revealed that their central neurexin-binding loops (NL1 395–402) are identical (Supplementary Fig. 6 online), and the surrounding small loops bear differences. NL1 and NL4 differ only slightly (NL1 Tyr499 vs NL4 Phe463), explaining their close neurexin-binding affinities. The weaker NX1β-binding affinity of NL3 can be attributed to the Tyr-to-His substitution at the NL1 Tyr295 position, where a hydrophobic sidechain is required for positioning the 294–297 loop for contacting NX1β. NL2 differs markedly from other neuroligins by a Gly-to-Gln substitution (NL1 Gly500 vs NL2 Gln475). In the NL1-NX1β complex, NL1 Gly500 faces the NX1β surface closely, and cannot be substituted by any residue with a sidechain, which would conflict with NX1β Ser239. Hence, structural rearrangement would be required in NL2 to accommodate Gln475 when binding neurexins. This would be unfavorable because the flanking residues interact extensively with NX1β in the complex. Our structure therefore suggests NL2 is not an optimal ligand for neurexins.

### Effects of splice sites on NL1-NX1β interaction

Of the three alternative spice sites harbored in the complex, the sites A and site B inserts of NL1 have been shown to reduce NL1-NX1β binding by 2–5 fold[20], whereas the SS#4 insert in neurexins nearly blocks the neuroligin-neurexin association[26,27]. Our structure indicates that site A of NL1 is more than 25Å from the edge of the NL1-NX1β interface, and is therefore unlikely to interfere with the neuroligin-neurexin association (Fig. 4a). In comparison, site B of NL1 is only ~10 Å from the edge of the interface, and is more likely to interfere with NL1-NX1β binding.

To determine how the site B insert of NL1 produces its inhibitory effect, we used isothermal titration calorimetry to compare the thermodynamic profiles of NL1, with and without the site B insert (NL1-ΔA *vs* NL1-ΔAΔB), in binding to NX1β (Fig. 4b and 4c). The measured affinities for NL1-ΔA/NX1β and NL1-ΔAΔB/NX1β are 430 nM and 93 nM, respectively.

NIH-PA Author Manuscript

NIH-PA Author Manuscript

NIH-PA Author Manuscript

Both binding events are enthalpy-driven, and are entropically unfavorable. The Δ*H* value of approximately −20 kcal $mol^{-1}$ is in agreement with the number of salt bridges and hydrogen bonds observed in the complex. Comparing the two thermodynamic profiles revealed that the site B insert produced an enthalpic loss (Δ*H* difference ~1.4 kcal $mol^{-1}$), but an entropic gain (TΔ*S* difference ~0.5 kcal $mol^{-1}$). There are two possible ways that the site B insert, which is near the NL1-NX1β interface, exerts its negative influence on binding. One possibility is steric hindrance: bringing the two proteins together limits the flexibility of the insert, resulting an entropic loss. Such a possibility does not agree with our thermodynamic data which show that the site B insert brings an entropic gain. The other possibility is that the site B insert disturbs/weakens an existing hydrogen bond/salt bridge. This possibility is consistent with the thermodynamic data: the enthalpic loss is due to bond-breaking and the associated entropic gain is due to increased conformational flexibility.

Consistent the second possibility, analyzing the NL1-NX1β structure revealed that the NL1 site B insert can interfere with an adjacent, dynamic salt bridge between NL1 Glu297 and NX1β Arg109. In our complex structure without the NL1 site B insert, the NX1β Arg109 sidechain show no electron density beyond Cβ, indicating it is flexible (Supplementary Fig. 7 online), but in its low-energy, extended conformation, both the Nη1 and Nε atoms of NX1β Arg109 are at appropriate distances from the carboxyl group of NL1 Glu297 to form a salt bridge. NL-neurexin interactions were previously shown to be electrostatically driven19. Mutation of E297A (combined with a remote K306A mutation that is unlikely relevant) has been reported to reduce NL1 binding to NX1β by 5-fold[20], supporting the existence of this salt bridge. Given the flexibility of NX1β Arg109, the correct conformation and the availability of NL1 Glu297 become important for the energetics of this salt bridge. In NL1 without the site B insert, Glu297 is held inflexible in a very tight turn; in NL1 with the site B insert (298–306) present, the insert, which is next to Glu297, would likely release this tight turn conformation and result in increased flexibility of Glu297, thus destabilizing the salt bridge with NX1β Arg109. The effect of mutating Glu297 to alanine in NL1 without insert B20 is similar to that of adding insert B (Fig. 4), each reduces binding by ~5 fold, further supporting that insert B acts though modulating the NL1 Glu297-NX1β salt bridge. Interestingly, the inhibitory effect of the NL1 site B insert appears to be augmented by the presence of the N-linked glycosylation in the middle of the insert residues[23]. This is perhaps because the N-linked glycan, with its large size, can restrain the conformation of the insert and adjacent residues, including Glu297, decreasing the possibility that NL1 Glu297 will achieve the conformation that allows salt bridge formation with NX1β Arg109.

Analysis of the structural elements around NX1β SS#4 suggest the SS#4 insert may use a similar mechanism to that of the NL1 site B insert to modulate NL1-neurexin recognition. This insert site is distant from the main NL1-NX1β binding interface, and is unlikely to act through steric hindrance. However, it is immediately adjacent to NX1β Arg232, which forms a salt bridge with NL1 Asp387 in the complex (Fig. 3). An insertion of 30 amino acids between Ala200 and Gly231 is likely to alter the conformation of NX1β Arg232, resulting in the loss or weakening of this salt bridge. Because incorporating the SS#4 insert reduces NL1-NX1β binding to an immeasurable level, direct thermodynamic evidence is unavailable for this supposition.

## Effects of the autism-related neuroligin mutations

Aberrant neuroligin genes have been linked to autism[11,15,16,31], but it remains unclear how the point mutations of neuroligins are related to the genesis of the disease. An NL3 mutation, R451C, and three NL4 mutations, G99S, K378R and V403M, located in the CLD domain, have been found in autistic patients[11,15]. These residues, corresponding to Arg473, Asp106, Lys414, and Val439 of NL1 respectively, are highly conserved except NL1 Asp106 (Supplementary Fig. 6 online). An inspection of the locations of these residues in the NL1-

NIH-PA Author Manuscript

NIH-PA Author Manuscript

NIH-PA Author Manuscript

NX1β complex indicates that they are distant from the neuroligin-neurexin interface and the neuroligin dimer interface, so are unlikely to affect neuroligin-neurexin binding or neuroligin dimerization (Fig. 5). All but Asp106 are largely buried beneath the protein surface in NL1. This is unexpected, as most of these residues, in particular, Lys414 and Arg473, are large hydrophilic residues. The buried nature indicates that most of the autism mutations in neuroligins compromise structural integrity. The mutations most likely result in insufficient folding, secretion or viability of the specific types of neuroligins, which would alter their functions at the synapse.

## Discussion

In this paper, we have determined the structure of the complex between the NL1 CLD and the NX1β LNS domain. We found that the neuroligin-neurexin association is highly hydrophilic, $Ca^{2+}$-mediated and water-supplemented, enabling it to be easily affected by a variety of factors such as ionic strength, $Ca^{2+}$ concentration, amino acid substitution and proximal splice inserts.

With respect to $Ca^{2+}$, the unexpected $Ca^{2+}$ binding site in NX1β, but not in NL1, is consistent with recent mutagenesis studies showing that mutations of NX1β residues disrupt $Ca^{2+}$-dependent postsynaptic protein clustering and neuroligin binding[25]. It is also consistent with the identification of a $Ca^{2+}$ binding site in the second LNS domain of NX1α[29], supporting the LNS domain as a common $Ca^{2+}$ binding module.

With respect to alternative splicing, such splicing is widely used in generating molecular diversity for receptor-ligand recognition, and the mechanisms by which splicing modulates recognition are only beginning to emerge. A recent study revealed that drosophila Dscam, a protein implicated in neural wiring, uses splice variant-specific sequences to form homophilic interactions with each other[32], unlike neurexins/neuroligins in which splice sites appear to interfere indirectly from outside the binding interface. This fundamental difference is based on different natures of splicing: the splicing of Dscam generates mutually exclusive, but inter-replaceable regions that are essential parts of the structure, whereas the splicing of neuroligins and neurexins generates inserts or deletions that are not essential to structural integrity. It was estimated that 60% of the human genes have two or more splicing variants[33], in which the insertion/deletion–type splicing represented by neuroligins and neurexins is predominant[33]. Since the minimal transcript is functional in most splicing cases, most of the extra inserts/deletions should be not essential to the structural integrity of and should extend from the core scaffold, as observed in neuroligins and neurexins. Therefore, regulating protein-protein recognition by modulating the strength of the interactions, especially salt bridges, at the edges of protein-protein interfaces, as represented by NL1 site B and neurexin SS#4, may be a general mechanism for a large pool of alternative splicing-regulated biological events.

Our NL1-NX1β structure reveals how minor sequence variations among neuroligins can determine their different NX1β-binding capacities. In particular, NL2, because its Gln475 substitutes for NL1 Gly500, is sterically incompatible with the neuroligin-binding surface of neurexins. This suggests that neurexins are unlikely to serve as NL2 receptors, and favors the opinion that NL1 and NL2 have different functional roles [2,3,34]. Our structure also suggests that most of the point mutations found in autism patients are structurally disruptive, likely compromising the synthesis of functional neuroligins. Consistent with our analysis, the NL3 R451C mutant has been demonstrated to be defective in cell-surface transport [8,9,35]. Intriguingly, a recent study of NL3 mutant mice suggested that NL3 R451C is a gain-of-function mutation[36]. The exact consequences of this mutation should be further addressed both structurally and functionally.

NIH-PA Author Manuscript

NIH-PA Author Manuscript

NIH-PA Author Manuscript

# METHODS

## Constructs and mutagenesis

The coding sequence of the NL1 extracellular CLD domain (residues 26–638) was cloned adjacent to an N-terminal 7-His tag in pAcGP67A (Pharmingin). The coding sequence for the NX1β LNS domain (residues 82–292), devoid of splice insert (residues 201–230), was cloned adjacent to a C-terminal 7-His tag, also in pAcGP67A. A GST-fusion cleavable NX1β construct with no His-tag was prepared using pET-49 (Novagen). Mutagenesis of NL1 and NX1β was carried out using overlap extension PCR, based on pAcGP67A-NL1 and pET-49-NX1β constructs, respectively. All constructs and mutations were verified by DNA sequencing.

## Protein preparation

His-tagged NL1, its mutants, and NX1β were prepared from baculovirus-infected insect cells. Recombinant baculovirus was produced by co-transecting sf9 cells with the pAcGP67A constructs and linearized baculovirus DNA (BacVector-3000, EMD). After amplification, the viruses were used to infect 1–6 liters of Hi5 cells at a density of $1.8\times10^6$ cells $ml^{-1}$ in HyQ SFX media (HyClone). Cell cultures were allowed to progress for 66 hours before being harvested by centrifugation. The proteins in the supernatant were captured by Ni-NTA resin and eluted with 200mM imidazole pH 7.5. They were further purified with size exclusion columns equilibrated with HBS buffer (10 mM Hepes, 150 mM NaCl, pH 7.5).

Non-His-tagged NX1β and its mutants were expressed as intracellular soluble GST fusion proteins from rosetta-gami2 E. coli cells (Novagen) induced at 25°C. Proteins were purified with glutathione-agarose column and gel filtration, and cleaved with HRV-3C protease overnight. The cleaved NX1β proteins were passed through a second glutathione-agarose column to separate uncleaved proteins, and further purified by a second gel filtration column.

## Crystallization and X-ray data collection

NL1 and NX1β proteins were concentrated to 10 mg $ml^{-1}$ in HBS with 5 mM $CaCl_2$, and combined at 3:1 ratio (v/v) for crystallization. Crystals were obtained through sitting-drop vapor-diffusion. The drops contained equal volumes of the protein and the reservoir solution (1.0 M sodium citrate, 0.1M sodium cacodylate, pH 6.5, 0.2 M NaCl, 10 mM $CaCl_2$). X-ray diffraction was measured at 0.9797 Å wavelength at beamlines 22-BM-C and 21-ID-D at the Advanced Photon Source (APS), Argonne, IL. Crystals were cryoprotected before being flashcooled to 100K with the presence of 10% (v/v) glycerol in the mother liquor. The data were indexed, integrated and scaled with HKL2000[37]. To prevent $Ca^{2+}$ from being chelated by citrate, a separate cryoprotecting solution with citrate replaced by acetate and a higher $Ca^{2+}$ concentration (3 M sodium acetate, 0.1 M sodium cacodylate, pH 6.5, 0.1 M $CaCl_2$, 10% (v/v) glycerol) was used to gradually adapt the crystals before they were flashcooled for X-ray diffraction.

## Structure determination and refinement

The structure was determined using the molecular replacement program PHASER38, with mouse AChE (PDB ID 1N5M) and free NX1β (PDB ID 1C4R) as search models. The model of the complex was rebuilt using the program O39, and refined using CNS40. In the final model, each NL1 contains two N-linked glycans (Asn109 and Asn547) with well-defined electron density; a third potential CLD glycosylation site, Asn343, was mutated to glutamine to facilitate crystallization. In the Ramachandran plot, 85.0 %, 14.4 %, 0.6 %, and 0 % of the

NIH-PA Author Manuscript

NIH-PA Author Manuscript

NIH-PA Author Manuscript

residues fall in favored, allowed, generally allowed, and disallowed regions, respectively. The statistics of data collection and refinement is summarized in Table 1.

### His-tag pull-down assays

Small columns loaded with 0.5 ml Ni-NTA agarose beads (bed volume ~0.25 ml) were washed with binding buffer (20 mM Hepes, pH 7.5, 10 mM CaCl2). Equal amounts of N-terminally His-tagged NL1 proteins (0.2 ml at 0.8 mg $ml^{-1}$) were then loaded to the columns. The columns were washed with 2 ml binding buffer. The His-tag-free NX1β and its mutants, cleaved from GST-fusion protein, were buffer-exchanged into the binding buffer with gel filtration, adjusted to equal concentrations (0.5 mg $ml^{-1}$), and then loaded in equal amounts (0.5 ml) onto the NL1-bound columns, respectively. 2 ml binding buffer was applied to wash off unbound NX1β proteins. The retained NX1β proteins, together with NL1 proteins, were then eluted off the Ni-NTA columns with 0.5 ml 0.2 M imidazole, pH 7.5 in HBS, and analyzed with SDS-PAGE.

### Isothermal Titration Calorimetry

Calorimetric titrations were carried out on a VP-ITC calorimeter (MicroCal, Northhampton, MA) at 30°C and the data were processed with MicroCal Origin 5.0 software. The protein concentration was determined by the bicinchoninic acid assay with bovine serum albumin as the standard (Pierce Rockford, IL). For measuring NL1-NX1β interactions, the proteins purified from insect cells were buffer-exchanged into an identical lot of binding buffer (20mM Hepes, pH7.5, 10mM $CaCl_2$) using gel filtration to control buffer heat dilution effects. Prior to each titration, protein samples were degassed for 10 minutes. The NX1β proteins were then added to NL1 over the course of numerous injections to the point that NL1 was fully saturated. For measuring binding interactions between NX1β and $Ca^{2+}$, native NX1β was added to a final concentration of 50mM EDTA, pH 8.0, to remove residual $Ca^{2+}$ potentially derived from cell culture. The protein was then buffer exchanged to 20mM Hepes, pH 7.5 using gel filtration. A $CaCl_2$ solution was prepared by dissolving $CaCl_2$ directly into the same 20mM Hepes buffer, and was then added to NX1β during the course of titration.

## Supplementary Material

Refer to Web version on PubMed Central for supplementary material.

## Acknowledgments

We thank E.M. Silinsky for critically reading the manuscript. X.H. is supported by Brain Tumor Society and the NIH grant 1R01GM078055. The Structural Biology Facility is supported by the R.H. Lurie Comprehensive Cancer Center of Northwestern University. Data were collected at Southeast Regional Collaborative Access Team (SER-CAT) beamline 22-BM-C and Life Sciences Collaborative Access Team (LS-CAT) beamline 21-ID-D at APS, Argonne National Laboratory.

## References

1. Craig AM, Graf ER, Linhoff MW. How to build a central synapse: clues from cell culture. Trends Neurosci 2006;29:8–20. [PubMed: 16337695]
2. Chih B, Engelman H, Scheiffele P. Control of excitatory and inhibitory synapse formation by neuroligins. Science 2005;307:1324–1328. [PubMed: 15681343]
3. Chubykin AA, et al. Activity-dependent validation of excitatory versus inhibitory synapses by neuroligin-1 versus neuroligin-2. Neuron 2007;54:919–931. [PubMed: 17582332]

NIH-PA Author Manuscript

NIH-PA Author Manuscript

NIH-PA Author Manuscript


4. Graf ER, Zhang X, Jin SX, Linhoff MW, Craig AM. Neurexins induce differentiation of GABA and glutamate postsynaptic specializations via neuroligins. Cell 2004;119:1013–1026. [PubMed: 15620359]
5. Scheiffele P, Fan J, Choih J, Fetter R, Serafini T. Neuroligin expressed in nonneuronal cells triggers presynaptic development in contacting axons. Cell 2000;101:657–669. [PubMed: 10892652]
6. Song JY, Ichtchenko K, Sudhof TC, Brose N. Neuroligin 1 is a postsynaptic cell-adhesion molecule of excitatory synapses. Proc Natl Acad Sci U S A 1999;96:1100–1105. [PubMed: 9927700]
7. Varoqueaux F, et al. Neuroligins determine synapse maturation and function. Neuron 2006;51:741–754. [PubMed: 16982420]
8. Chih B, Afridi SK, Clark L, Scheiffele P. Disorder-associated mutations lead to functional inactivation of neuroligins. Hum Mol Genet 2004;13:1471–1477. [PubMed: 15150161]
9. Comoletti D, et al. The Arg451Cys-neuroligin-3 mutation associated with autism reveals a defect in protein processing. J Neurosci 2004;24:4889–4893. [PubMed: 15152050]
10. Feng J, et al. High frequency of neurexin 1beta signal peptide structural variants in patients with autism. Neurosci Lett 2006;409:10–13. [PubMed: 17034946]
11. Jamain S, et al. Mutations of the X-linked genes encoding neuroligins NLGN3 and NLGN4 are associated with autism. Nat Genet 2003;34:27–29. [PubMed: 12669065]
12. Laumonnier F, et al. X-linked mental retardation and autism are associated with a mutation in the NLGN4 gene, a member of the neuroligin family. Am J Hum Genet 2004;74:552–557. [PubMed: 14963808]
13. Szatmari P, et al. Mapping autism risk loci using genetic linkage and chromosomal rearrangements. Nat Genet 2007;39:319–328. [PubMed: 17322880]
14. Talebizadeh Z, et al. Novel splice isoforms for NLGN3 and NLGN4 with possible implications in autism. J Med Genet 2006;43:e21. [PubMed: 16648374]
15. Yan J, et al. Analysis of the neuroligin 3 and 4 genes in autism and other neuropsychiatric patients. Mol Psychiatry 2005;10:329–332. [PubMed: 15622415]
16. Lise MF, El-Husseini A. The neuroligin and neurexin families: from structure to function at the synapse. Cell Mol Life Sci 2006;63:1833–1849. [PubMed: 16794786]
17. Missler M, Hammer RE, Sudhof TC. Neurexophilin binding to alpha-neurexins. A single LNS domain functions as an independently folding ligand-binding unit. J Biol Chem 1998;273:34716–34723. [PubMed: 9856994]
18. Rudenko G, Nguyen T, Chelliah Y, Sudhof TC, Deisenhofer J. The structure of the ligand-binding domain of neurexin Ibeta: regulation of LNS domain function by alternative splicing. Cell 1999;99:93–101. [PubMed: 10520997]
19. Comoletti D, et al. Characterization of the interaction of a recombinant soluble neuroligin-1 with neurexin-1beta. J Biol Chem 2003;278:50497–50505. [PubMed: 14522992]
20. Comoletti D, et al. Gene selection, alternative splicing, and post-translational processing regulate neuroligin selectivity for beta-neurexins. Biochemistry 2006;45:12816–12827. [PubMed: 17042500]
21. Comoletti D, et al. Synaptic arrangement of the neuroligin/beta-neurexin complex revealed by X-ray and neutron scattering. Structure 2007;15:693–705. [PubMed: 17562316]
22. Nguyen T, Sudhof TC. Binding properties of neuroligin 1 and neurexin 1beta reveal function as heterophilic cell adhesion molecules. J Biol Chem 1997;272:26032–26039. [PubMed: 9325340]
23. Boucard AA, Chubykin AA, Comoletti D, Taylor P, Sudhof TC. A splice code for trans-synaptic cell adhesion mediated by binding of neuroligin 1 to alpha- and beta-neurexins. Neuron 2005;48:229–236. [PubMed: 16242404]
24. Chih B, Gollan L, Scheiffele P. Alternative splicing controls selective trans-synaptic interactions of the neuroligin-neurexin complex. Neuron 2006;51:171–178. [PubMed: 16846852]
25. Graf ER, Kang Y, Hauner AM, Craig AM. Structure function and splice site analysis of the synaptogenic activity of the neurexin-1 beta LNS domain. J Neurosci 2006;26:4256–4265. [PubMed: 16624946]
26. Ichtchenko K, et al. Neuroligin 1: a splice site-specific ligand for beta-neurexins. Cell 1995;81:435–443. [PubMed: 7736595]

NIH-PA Author Manuscript

NIH-PA Author Manuscript

NIH-PA Author Manuscript


27. Ichtchenko K, Nguyen T, Sudhof TC. Structures, alternative splicing, and neurexin binding of multiple neuroligins. J Biol Chem 1996;271:2676–2682. [PubMed: 8576240]
28. Bourne Y, Taylor P, Marchot P. Acetylcholinesterase inhibition by fasciculin: crystal structure of the complex. Cell 1995;83:503–512. [PubMed: 8521480]
29. Sheckler LR, Henry L, Sugita S, Sudhof TC, Rudenko G. Crystal structure of the second LNS/LG domain from neurexin 1alpha: Ca2+ binding and the effects of alternative splicing. J Biol Chem 2006;281:22896–22905. [PubMed: 16772286]
30. Lo Conte L, Chothia C, Janin J. The atomic structure of protein-protein recognition sites. J Mol Biol 1999;285:2177–2198. [PubMed: 9925793]
31. Dean C, Dresbach T. Neuroligins and neurexins: linking cell adhesion, synapse formation and cognitive function. Trends Neurosci 2006;29:21–29. [PubMed: 16337696]
32. Meijers R, et al. Structural basis of Dscam isoform specificity. Nature 2007;449:487–491. [PubMed: 17721508]
33. Kim E, Magen A, Ast G. Different levels of alternative splicing among eukaryotes. Nucleic Acids Res 2007;35:125–131. [PubMed: 17158149]
34. Prange O, Wong TP, Gerrow K, Wang YT, El-Husseini A. A balance between excitatory and inhibitory synapses is controlled by PSD-95 and neuroligin. Proc Natl Acad Sci U S A 2004;101:13915–13920. [PubMed: 15358863]
35. Chubykin AA, et al. Dissection of synapse induction by neuroligins: effect of a neuroligin mutation associated with autism. J Biol Chem 2005;280:22365–22374. [PubMed: 15797875]
36. Tabuchi K, et al. A neuroligin-3 mutation implicated in autism increases inhibitory synaptic transmission in mice. Science 2007;318:71–76. [PubMed: 17823315]
37. Otwinowski Z, Minor W. Processing of X-ray diffraction data collected in oscillation mode. Methods Enzymol 1997;276:307–326.
38. McCoy AJ, et al. Phaser crystallographic software. J Appl Cryst 2007;40:658–674. [PubMed: 19461840]
39. Jones TA, Zou JY, Cowan SW, Kjeldgaard M. Improved methods for binding protein models in electron density maps and the location of errors in these models. Acta Crystallogr. A 1991;47:110–119. [PubMed: 2025413]
40. Brunger AT, et al. Crystallography & NMR system: A new software suite for macromolecular structure determination. Acta Crystallogr. D 1998;54:905–921. [PubMed: 9757107]

NIH-PA Author Manuscript
NIH-PA Author Manuscript
NIH-PA Author Manuscript



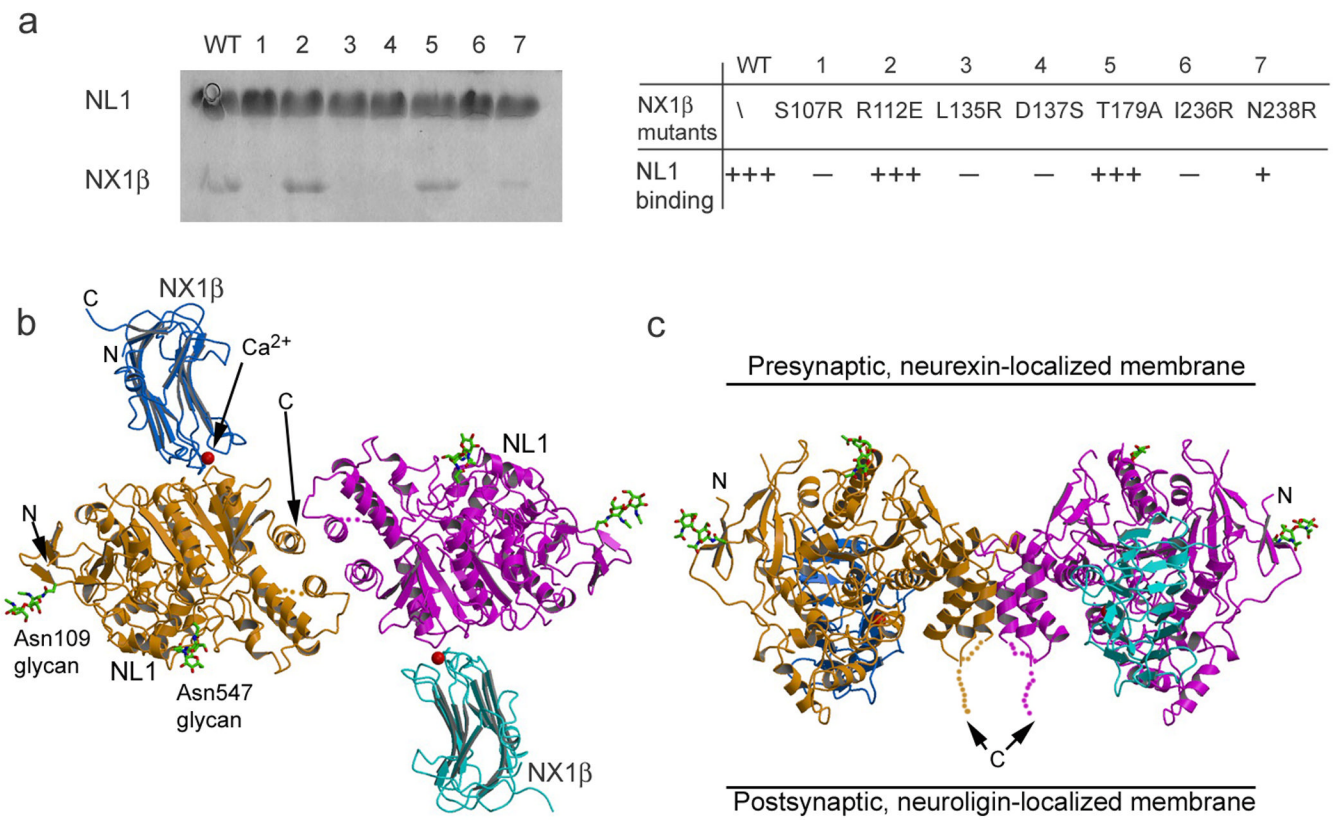


**Figure 1. Structure of the NL1-NX1β complex**

(**a**) His-tag pulldown assay showing effects of mutagenesis of NX1β surface residues on NL1 binding. The gel is Coomassie-stained SDS-PAGE, with upper bands being His-tagged NL1 attached to Ni-NTA resin, and lower bands being non-His-tagged NX1β mutants retained by NL1. (**b**) The 2:2 NL1-NX1β complex in ribbons model, viewed from the direction of NX1β-localized membrane. NL1 is colored in orange and pink, NX1β in blue and cyan. $Ca^{2+}$ ions are depicted as red balls. (**c**) The complex viewed from the side.

NIH-PA Author Manuscript
NIH-PA Author Manuscript
NIH-PA Author Manuscript



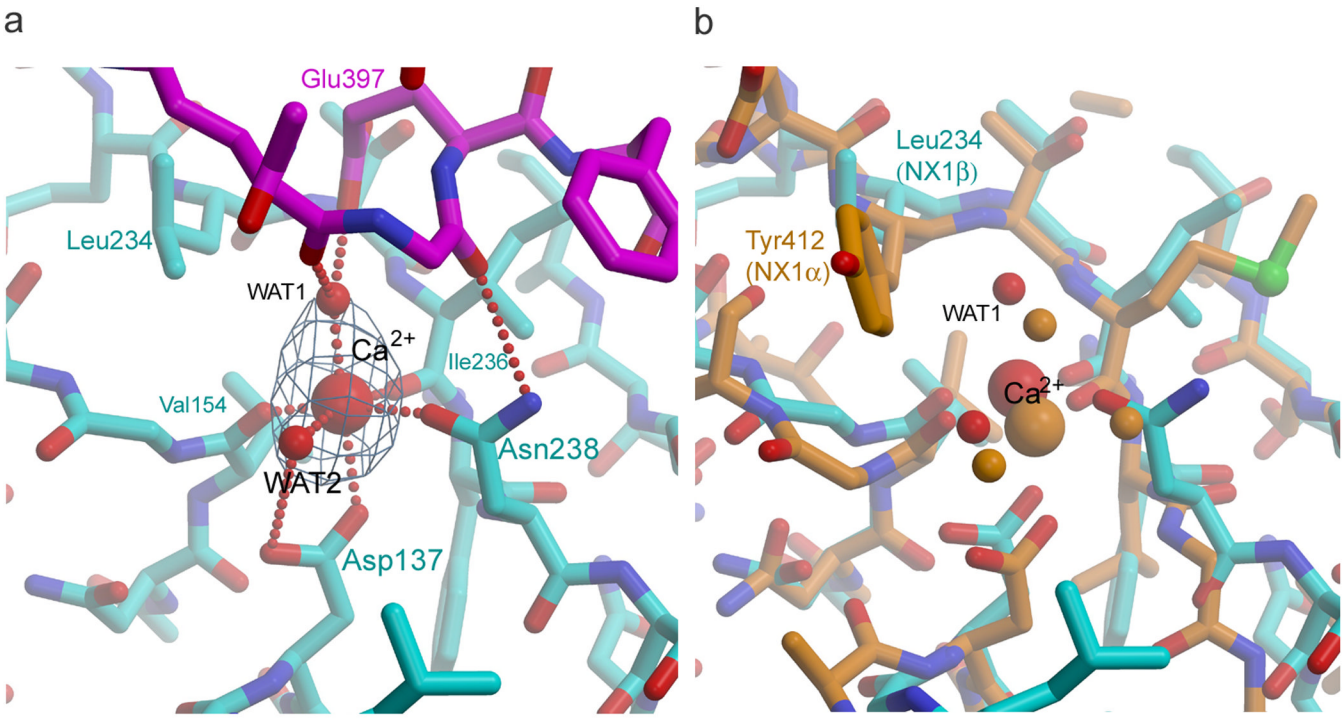


**Figure 2. The $Ca^{2+}$ binding site in the NL1-NX1β complex**

(**a**) Coordination of the $Ca^{2+}$ and its effect on NL1-NX1β interaction. NX1β is colored cyan, and NL1 colored pink. $Ca^{2+}$ and waters are shown as red balls. Hydrogen bonds and $Ca^{2+}$-oxygen interactions are shown as dashed red lines. Fo-Fc electron density calculated with the $Ca^{2+}$ and waters omitted from the model is shown contoured at 4.5σ. The $Ca^{2+}$ ion is octahedrally coordinated by four protein oxygen atoms from NX1β and two water molecules. WAT1 is bonded to both the $Ca^{2+}$ and two NL1 oxygen atoms. The NX1β Asn238 sidechain is both bonded to the $Ca^{2+}$ and to the NL1 mainchain. (**b**) Overlaying the structures of the $Ca^{2+}$ bound to NX1β ($Ca^{2+}$ as red ball and NX1β as cyan sticks) with the $Ca^{2+}$ bound to NX1α-LNS2 (both $Ca^{2+}$ and NX1α colored in orange) shows that the $Ca^{2+}$ binding sites are in similar positions of the LNS domain. The major difference is that WAT1 in NX1β requires NL1 to be positioned, but the equivalent water in NX1α-LNS2's structure can be positioned by the sidechain of Tyr412.

NIH-PA Author Manuscript
NIH-PA Author Manuscript
NIH-PA Author Manuscript



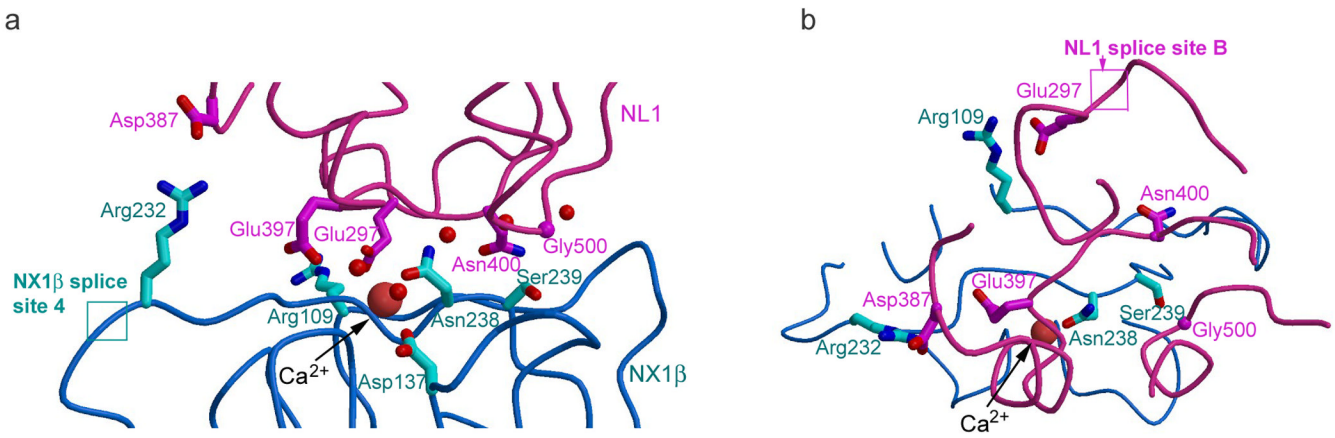


**Figure 3. The NL1-NX1β interface**

(**a**) Side view. NL1 and NX1β backbones are shown as coils. The sidechains of the important residues in NL1-NX1β interaction are shown as sticks. Waters and the $Ca^{2+}$ are shown as red balls. The position of NX1β splice site 4 is shown as a cyan square, and is near the salt bridge between NL1 Asp387 and NX1β Arg232. (**b**) View from the NL1 direction. The position of NL1 splice site B is shown as a pink square, and is near the salt bridge between NL1 Glu297 and NX1β Arg109.

NIH-PA Author Manuscript
NIH-PA Author Manuscript
NIH-PA Author Manuscript



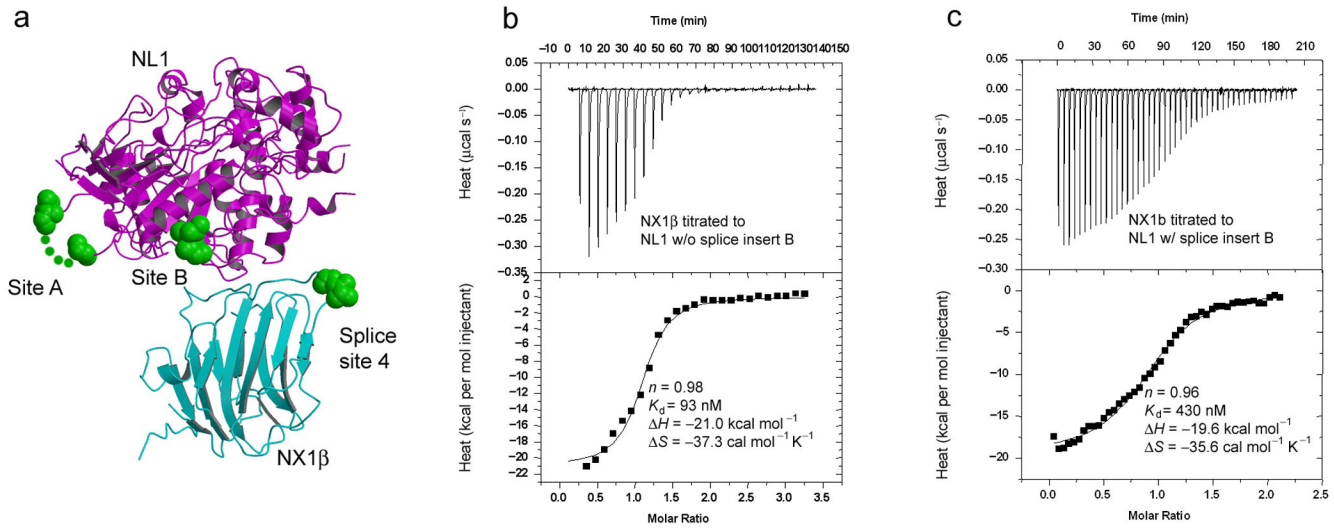


**Figure 4. Alternative splice sites in the NL1-NX1β complex**

(**a**) The locations of the NL1 sites, A and B, and NX1β SS#4 on the surface of the complex. Each residue immediately adjacent to the potential insert is colored green and shown in CPK representation. (**b**) Calorimetric titration between NL1 without the site B insert and NX1β. (**c**) Calorimetric titration between NL1 with the site B insert and NX1β. The NL1 protein does not have the site A insert and the NX1β protein does not have the SS#4 insert.

NIH-PA Author Manuscript
NIH-PA Author Manuscript
NIH-PA Author Manuscript



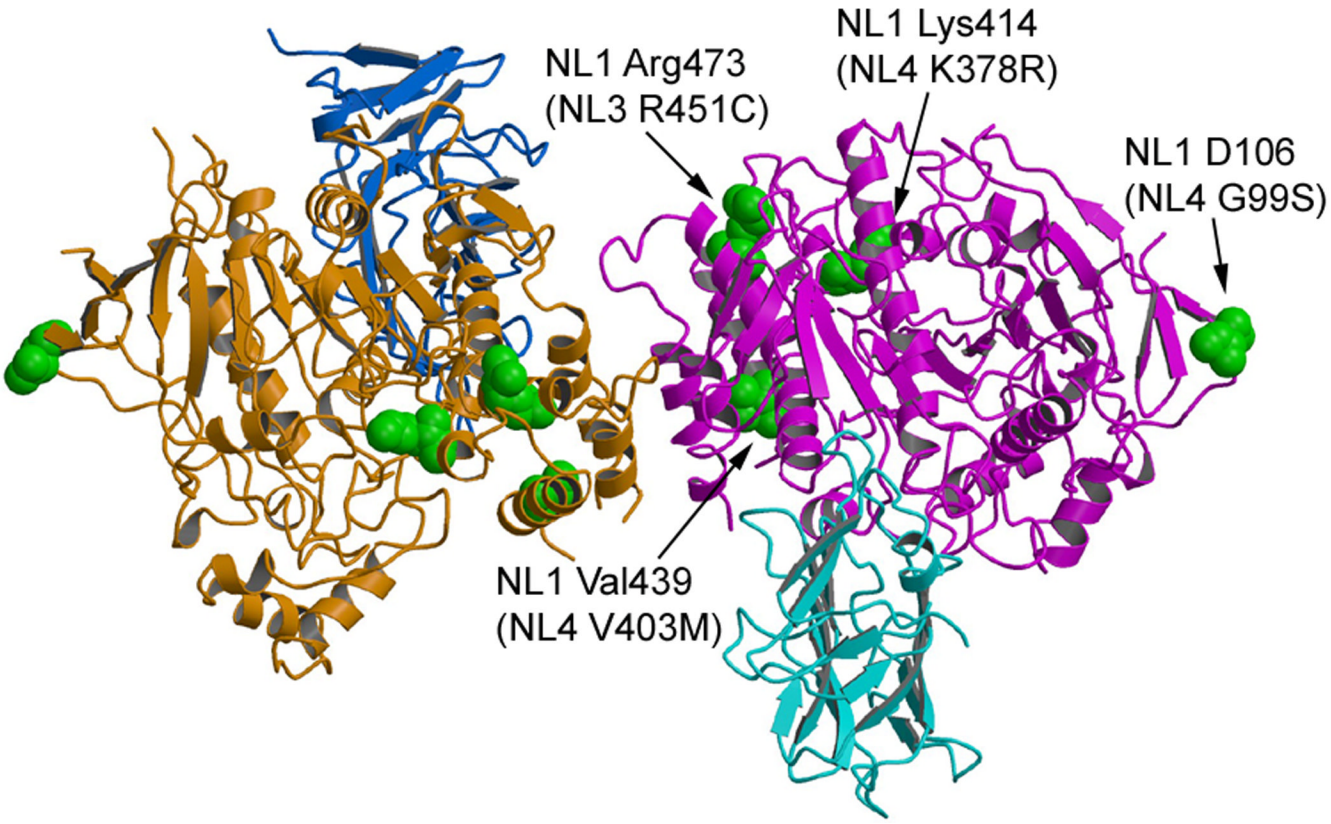


**Figure 5. Autism-related neuroligin point mutations**

The residues of mutations, NL1 Lys414 (corresponding to the NL4 K378R mutation), NL1 Arg473 (corresponding to the NL3 R451C mutation) and NL1 Val439 (corresponding to the NL4 V403M mutation), are colored in green and shown in CPK representation, and are mapped on the NL1-NX1β complex (ribbons). Note that these residues are away from the binding and dimerization interfaces, and are mostly buried.

NIH-PA Author Manuscript
NIH-PA Author Manuscript
NIH-PA Author Manuscript



**Table 1**

Data collection and refinement statistics

| | NX1β-NL1 in citrate ($Ca^{2+}$ chelated) | NX1β-NL1 adapted to acetate ($Ca^{2+}$ un-chelated) |
|---|---|---|
| **Data collection** | | |
| Space group | $P2_12_12_1$ | $P2_12_12_1$ |
| Cell dimensions | | |
| *a*, *b*, *c* (Å) | 116.59, 125.40, 131.86 | 120.62, 127.38, 133.26 |
| α, β, γ (°) | 90, 90, 90 | 90, 90, 90 |
| Resolution (Å) | 50-2.4(2.5-2.4)* | 50-3.5 (3.6-3.5) |
| $R_{merge}$ | 0.062 (0.463) | 0.067 (0.441) |
| $I/\sigma I$ | 19.3(3.2) | 18.4 (4.0) |
| Completeness (%) | 97.5(96.9) | 99.6 (99.7) |
| Redundancy | 4.5(4.0) | 5.1(5.4) |
| **Refinement** | | |
| Resolution (Å) | 50-2.4 | |
| No. reflections | 76375 | |
| $R_{work}$ / $R_{free}$ | 0.243 / 0.261 | |
| No. atoms | | |
| Protein | 11414 | |
| Ion | 2 | |
| Water | 1552 | |
| *B*-factors ($Å^2$) | | |
| Protein | 61.1 | |
| Ion | 32.1 | |
| Water | 70.2 | |
| R.m.s. deviations | | |
| Bond length (Å) | 0.008 | |
| Bond angles (°) | 1.1 | |

*One crystal was used for each dataset. Values in parentheses are for highest-resolution shell.